Huang *et al.*
Natural Products and Bioprospecting (2026) 16:69
https://doi.org/10.1007/s13659-026-00624-0

Natural Products and Bioprospecting

ORIGINAL ARTICLE Open Access

Rapid exploration of anti-MRSA components from plants of *Salvia*

Huan Huang[1†], Zhao-Jie Wang[1†], Li-Yu Bai[1], Yue-Ming Jiang[1], Yan-Yan Zhu[1], Yun-Li Zhao[1*] and Xiao-Dong Luo[1,2*]

Abstract

Plants of *Salvia* are frequently used for treatment infections of boils and sores in Traditional Chinese medicine, which might inhibit microbial. In this work, the chemical constituents of the effective fractions were analyzed using UPLC-Q-TOF–MS, and multivariate analysis and network pharmacology were used to predict potential antibacterial substances and their mechanism. Moreover, against methicillin-resistant *Staphylococcus aureus* (MRSA) effect and pathway of bioactive compounds were validated by experiments in vitro and in vivo. Two unreported anti-MRSA compounds, miltirone and przewaquinone A were proposed and then validated by serial experiments. They acted as bactericides and biofilm scavengers, respectively, and both targeted on the cell membrane, causing leakage of contents and affecting intracellular metabolism, leading to bacterial death without significant toxicity. Furthermore, miltirone ameliorated skin wound infection caused by MRSA in mice, roughly equal to vancomycin. The research supported the traditional use of *Salvia* plants, and presented two potent bactericidal agents for further investigation.

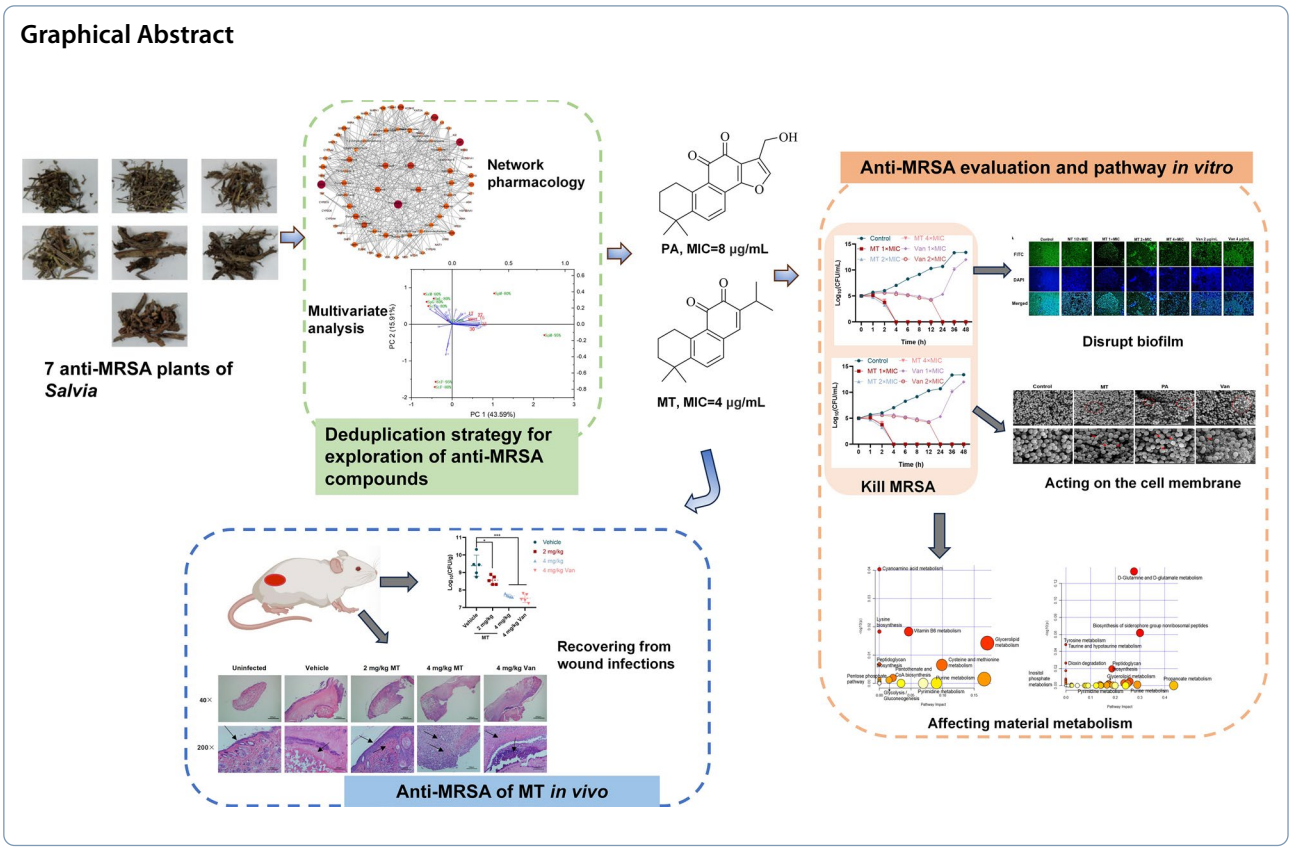
Keywords *Salvia*, Anti-MRSA, Miltirone, Przewaquinone A, Mechanism, In vitro and in vivo

†Huan Huang and Zhao-Jie Wang have contributed equally to this work.

*Correspondence:
Yun-Li Zhao
zhaoyunli@ynu.edu.cn
Xiao-Dong Luo
xdluo@ynu.edu.cn
Full list of author information is available at the end of the article

© The Author(s) 2026. **Open Access** This article is licensed under a Creative Commons Attribution 4.0 International License, which permits use, sharing, adaptation, distribution and reproduction in any medium or format, as long as you give appropriate credit to the original author(s) and the source, provide a link to the Creative Commons licence, and indicate if changes were made. The images or other third party material in this article are included in the article's Creative Commons licence, unless indicated otherwise in a credit line to the material. If material is not included in the article's Creative Commons licence and your intended use is not permitted by statutory regulation or exceeds the permitted use, you will need to obtain permission directly from the copyright holder. To view a copy of this licence, visit http://creativecommons.org/licenses/by/4.0/.

Springer



1 Introduction

Staphylococcus aureus is a common gram-positive pathogen [1, 2] that imposes a substantial healthcare burden, with tens of thousands of annual deaths attributed to *S. aureus* infections [3]. High mortality and incidence rates of bacteremia, bone infection, and endocarditis can be attributed to this factor. MRSA has high levels of resistance, and the efficacy of most antibiotics currently available in clinical practice is progressively decreasing [4]. In 2019, the direct impact of MRSA resulted in an estimated 10,000 fatalities [5]. Plants natural products are a crucial source of anti-MRSA drugs [6] and are an important strategy for overcoming bacterial resistance [7]. Then there is a high level of expectation for the extensive application of plant-derived antibacterial agents as effective remedies to address the current challenges of antibiotic resistance.

The *Salvia* genus of the Labiatae family is distributed mainly in southwest China [8]. The chemical constituents of this genus, including diterpenoids, triterpenoids, flavonoids and steroids exhibited therapeutic properties, such as anti-inflammatory, detumescent and efficacy against dysentery in Materia Medica (Ben-Cao-Shi-Yi in Chinese), which might be caused by *S. aureus* [9]. The anti-MRSA potential of seven plants was screened (Table S1), and different extracts of 7 *Salvia* plants showed anti-MRSA bioactivity with minimum inhibitory concentrations (MIC) ranging from 16 to 256 μg/ml (Table S2), which supposed the presence of same bioactive compounds in this genus. To avoid repeating isolation of the seven plants routinely, chemical compositions analysis of the bioactive fractions from each plants were carried out by UPLC-Q-TOF–MS, and then anti-MRSA bioactive compounds were predicted using multivariate analysis [10] and network pharmacology [11]. As a result, two unknown anti-MRSA compounds, miltirone (MT) and przewaquinone A (PA) were explored, and their anti-MRSA efficiency and pathway were validated in vitro and in vivo.

2 Results

2.1 Identification and quantification of compounds from bioactive plants

9 bioactive fractions from 7 *Salvia* plants were analyzed using UPLC-Q-TOF–MS, and the results of the TICs were shown in Fig. S1A and B. QC samples were used to assess the stability of the instrument, and three biological replicates in each group showed good repeatability (Fig. 1B). A total of 44 compounds were identified (Table 1), including 15 diterpenes, 9 flavonoids, and 13 triterpenes, in which

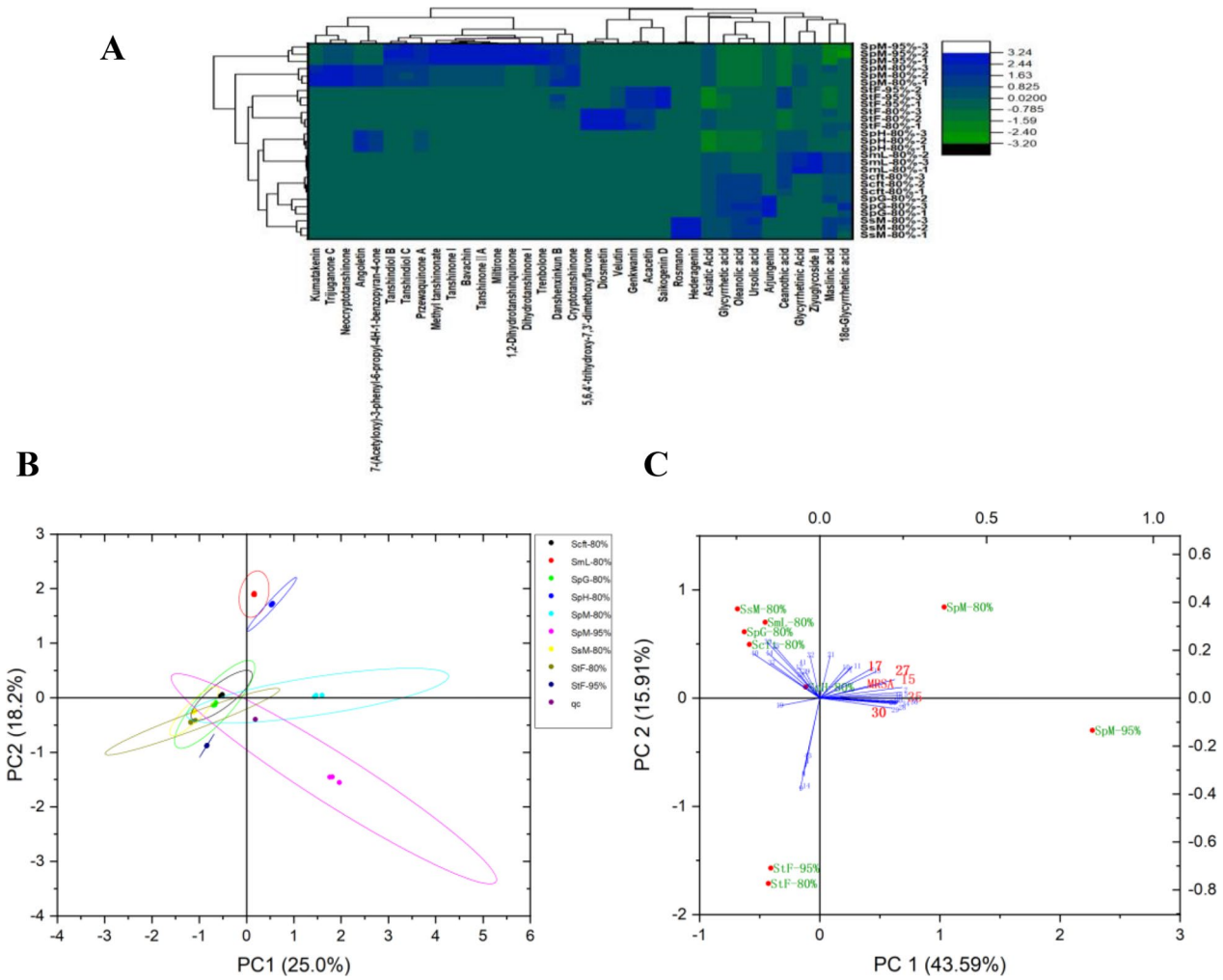


Fig. 1 **A** Heatmap. **B** Score plots. **C** Principal component analysis of correlations between compounds and anti-MRSA bioactivity

36 major compounds were quantified (Table S5). MS^1 exists mainly in the form of $[M+H]^+$, and the fragmentation pathway of przewaquinone A (**15**) was examined as an example (Fig. S3). The limits of detection (LOD) and quantification (LOQ) in Table S4 were determined using signal-to-noise ratios (S/N) of 3 and 10, respectively. The differences among the 9 fractions were visualized using the heatmap (Fig. 1A), and two principal components (Fig. 1B, C) explained 59.5% of the total variability. Then przewaquinone A (**15**), neocryptotanshinone (**17**), cryptotanshinone (**27**), dihydrotanshinone I (**30**), and miltirone (**35**) showed highly correlated to anti-MRSA bioactivity by PCA analysis.

2.2 Prediction of bioactivity components and mechanism by network pharmacology

The database predicted 739 targets for the 36 compounds and 794 targets for the anti-MRSA antibodies. Venn analysis revealed an overlap of 55 targets, indicating potential therapeutic targets (Fig. 2A). The protein–protein interaction (PPI) network (Fig. S4A) was constructed by importing these targets into the STRING database and visualizing them using Cytoscape 3.7.1., and then "disease-targeted drug target" network was constructed (Fig. 2B) to present common targets for compounds and diseases and predict potential bioactive compounds [11]. As a result, przewaquinone A (**15**), miltirone (**35**),

Table 1 Chemical constituents by UPLC-Q-TOF–MS analysis

No	RT (time)	ESI mode	Err (ppm)	m/z	MS/MS fragment ions	Molecular Formula	Compounds	References
1	4.45	$[M+H]^+$	− 0.95	315.0873	299.05, 257.04, 121.02	$C_{17}H_{14}O_6$	Kumatakenin	Standard
2	4.60	$[M+H]^+$	3.19	313.1081	373.16, 295.09, 267.10	$C_{18}H_{16}O_5$	Tanshindiol B	[12]
3	4.83	$[M-H]^-$	2.23	359.0780	161.02, 197.04, 135.04, 72.99	$C_{18}H_{16}O_8$	Rosmarinic acid	MSDIAL
4	4.89	$[M+H]^+$	2.11	331.0819	331.08	$C_{17}H_{14}O_7$	5,6,4′-trihydroxy-7,3′- dimethoxyflavone	Standard
5	4.90	$[M+H]^+$	2.87	313.1080	295.09, 267.10	$C_{18}H_{16}O_5$	Tanshindiol C	MSDIAL, GNPS
6	5.04	$[M+Na]^+$	1.22	329.1388	229.08, 197.05, 169.06, 141.06,	$C_{19}H_{20}O_5$	Columbianadin	MSDIAL
7	5.19	$[M+H]^+$	0.33	301.0708	258.05, 186.98, 163.03, 124.01	$C_{16}H_{12}O_6$	Diosmetin	MSDIAL
8	5.33	$[M+H]^+$	0.95	315.0866	300.06, 282.05, 187.14, 108.02	$C_{17}H_{14}O_6$	Velutin	MSDIAL
9	5.81	$[M+H]^+$	7.37	285.0778	242.05, 229.08, 187.03, 124.01	$C_{16}H_{12}O_5$	Genkwanin	MSDIAL
10	6.11	$[M+H]^+$	1.33	301.1438	283.13, 268.10, 265.12, 185.05	$C_{18}H_{20}O_4$	Angoletin	MSDIAL GNPS
11	6.11	$[M+Na]^+$	− 7.43	323.1254	309.10, 265.08, 250.10, 223.07	$C_{20}H_{18}O_4$	7-(Acetyloxy)-3-phenyl-6-propyl-4H-1-benzopyran-4-one	MSDIAL
12	6.48	$[M-H]^-$	3.77	345.1720	283.17, 227.10, 268.14	$C_{20}H_{26}O_5$	Rosmanol	Standard
13	6.66	$[M+H]^+$	4.10	341.1398	313.14, 281.08, 263.07	$C_{20}H_{20}O_5$	Trijuganone C	[13]
14	7.23	$[M-H]^-$	3.18	283.0621	268.03, 240.09, 151.00, 117.03, 107.01	$C_{16}H_{12}O_5$	Acacetin	MSDIAL [14]
15	7.23	$[M+H]^+$	− 2.57	311.1278	293.11, 275.10, 265.12	$C_{19}H_{18}O_4$	Przewaquinone A	Standard
16	7.33	$[M+H]^+$	1.80	389.1966	329.17, 311.16, 287.16	$C_{22}H_{28}O_6$	Quassin	MSDIAL
17	7.57	$[M+H]^+$	1.90	315.1597	297.15, 279.13, 254.09, 193.10	$C_{19}H_{22}O_4$	Neocryptotanshinone	Standard
18	7.84	$[M+H]^+$	7.08	339.1251	311.12, 279.10, 261.09, 233.09	$C_{20}H_{18}O_5$	Methyl tanshinonate	[15]
19	7.86	$[M+H]^+$	0.21	487.3419	469.33, 423.32, 405.31, 165.06, 119.08	$C_{30}H_{46}O_5$	Ceanothic acid	MSDIAL
20	7.95	$[M+H]^+$	0.00	281.1172	303.09, 235.11	$C_{18}H_{16}O_3$	Danshenxinkun B	MSDIAL [16]
21	8.13	$[M-H]^-$	0.82	487.3433	487.34, 227.21	$C_{30}H_{48}O_5$	Asiatic Acid	MADIAL
22	8.22	$[M+H]^+$	0.00	279.2319	262.22, 233.09, 95.08, 81.07, 67.05	$C_{18}H_{30}O_2$	Linolenic acid	MSDIAL
23	8.50	$[M+H]^+$	3.32	301.2172	259.16, 213.12, 163.07, 171.08	$C_{20}H_{28}O_2$	Sugiol	[13]
24	8.68	$[M-H]^-$	2.43	329.1766	285.18, 201.09	$C_{20}H_{26}O_4$	Carnosol	Standard
25	8.69	$[M+H]^+$	− 1.91	471.3469	453.23, 425.34, 189.16, 175.14, 95.08	$C_{30}H_{46}O_4$	Glycyrrhetic acid	MSDIAL [17]
26	8.78	$[M+H]^+$	3.05	277.0873	249.09, 178.07,141.06	$C_{18}H_{12}O_3$	Tanshinone I	Standard
27	8.98	$[M+H]^+$	2.39	297.1504	254.09, 221.09, 193.10	$C_{19}H_{20}O_3$	Cryptotanshinone	Standard [18]
28	9.18	$[M+Na]^+$	2.46	325.1442	297.14, 269.15, 193.100, 167.08,	$C_{20}H_{20}O_4$	Bavachin	MSDIAL
29	9.51	$[M+H]^+$	4.30	279.1028	261.09, 233.09, 205.10, 190.07	$C_{18}H_{14}O_3$	1,2-Dihydrotanshinquinone	Standard
30	9.52	$[M+H]^+$	4.66	279.1029	233.09, 261.09, 205.10	$C_{18}H_{14}O_3$	Dihydrotanshinone I	Standard
31	9.68	$[M-H]^-$	2.78	503.3392	-	$C_{30}H_{48}O_6$	Pygenic acid C	MSDIAL
32	10.12	$[M+H]^+$	4.24	471.3489	407.33, 247.16, 201.16, 119.08	$C_{30}H_{46}O_4$	Glycyrrhetinic Acid	MSDIAL
33	10.41	$[M-H]^-$	0.42	471.3482	471.34, 405.30	$C_{30}H_{48}O_4$	Maslinic acid	Standard
34	10.52	$[M+H]^+$	5.42	295.1345	277.12, 253.11, 46.06	$C_{19}H_{18}O_3$	Tanshinone IIA	Standard
35	10.95	$[M+H]^+$	1.77	283.1698	223.11, 179.08, 165.07	$C_{19}H_{22}O_2$	Miltirone	Standard
36	11.79	$[M+H]^+$	2.21	271.1699	241.12, 227.10, 199.07, 117.07	$C_{18}H_{22}O_2$	Trenbolone	MSDIAL [19]
37	12.79	$[M+H]^+$	0.44	457.3676	–	$C_{30}H_{48}O_3$	Oleanolic acid	MSDIAL, GNPS
38	12.79	$[M+Na]^+$	4.55	505.3547	–	$C_{30}H_{48}O_6$	Arjungenin	MSDIAL
39	12.87	$[M+Na]^+$	2.87	627.3685	–	$C_{35}H_{56}O_8$	Ziyuglycoside II	MSDIAL
40	12.92	$[M-H]^-$	1.70	469.3331	–	$C_{30}H_{46}O_4$	18α-Glycyrrhetinic acid	MSDIAL
41	13.37	$[M-H]^-$	2.76	471.3491	–	$C_{30}H_{48}O_4$	Hederagenin	MSDIAL
42	13.42	$[M-H]^-$	2.33	471.3491	471.34, 423.32	$C_{30}H_{48}O_4$	Pygenic acid A	MSDIAL
43	14.17	$[M+Na]^+$	− 3.23	495.3445	435.23, 205.15, 101.07, 45.03	$C_{30}H_{48}O_4$	Saikogenin D	MSDIAL
44	14.60	$[M-H]^-$	1.98	455.3540	407.33, 297.23, 48.82	$C_{30}H_{48}O_3$	Ursolic acid	Standard

RT retention time

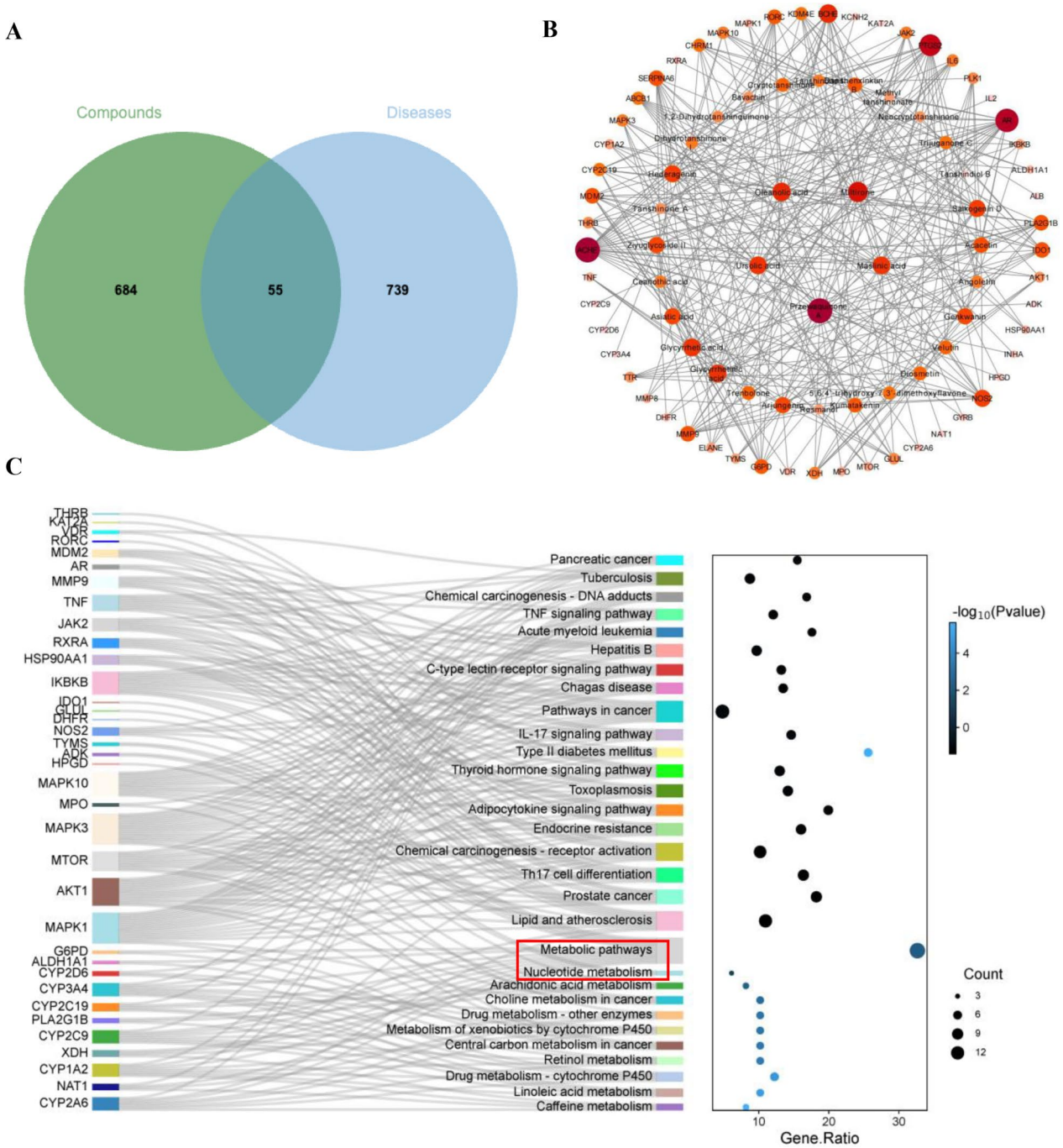


Fig. 2 **A** The Venn graph of the main components targets of biological fractions and anti-MRSA targets. **B** Potential effective compounds against MRSA. The color depth represented the importance of targets. **C** Sankey bubble chart of KEGG enrichment analysis

oleanolic acid (**37**), maslinic acid (**33**), and ursolic acid (**44**) were supposed to be bioactive components, in which unreported przewaquinone A (**15**) and miltirone (**35**) were selected for further investigation. Moreover, the KEGG analysis (Fig. 2C) showed that the main targets were enriched in nucleotide metabolism, linoleic acid metabolism, and arachidonic acid metabolism.

2.3 Miltirone and przewaquinone A acted as bactericide and removing biofilm

Przewaquinone A and miltirone showed good antibacterial bioactivity against multidrug-resistant gram-positive bacteria (Table S6) particularly against MRSA, and then a time-kill curve was used to evaluate the sterilization performances of them at 48 h (Fig. 3B, C). Miltirone exhibited excellent bactericidal bioactivity with the bacterial count under the detection limit at 1×, 2×, and 4×MIC after 4 h, while przewaquinone A completely killed the bacteria at an MIC of 4×after 24 h, showing advantage over vancomycin. In addition, both compounds inhibited growth of MRSA in a dose-dependent manner (Fig. 3D, E). Moreover, they showed scavenging

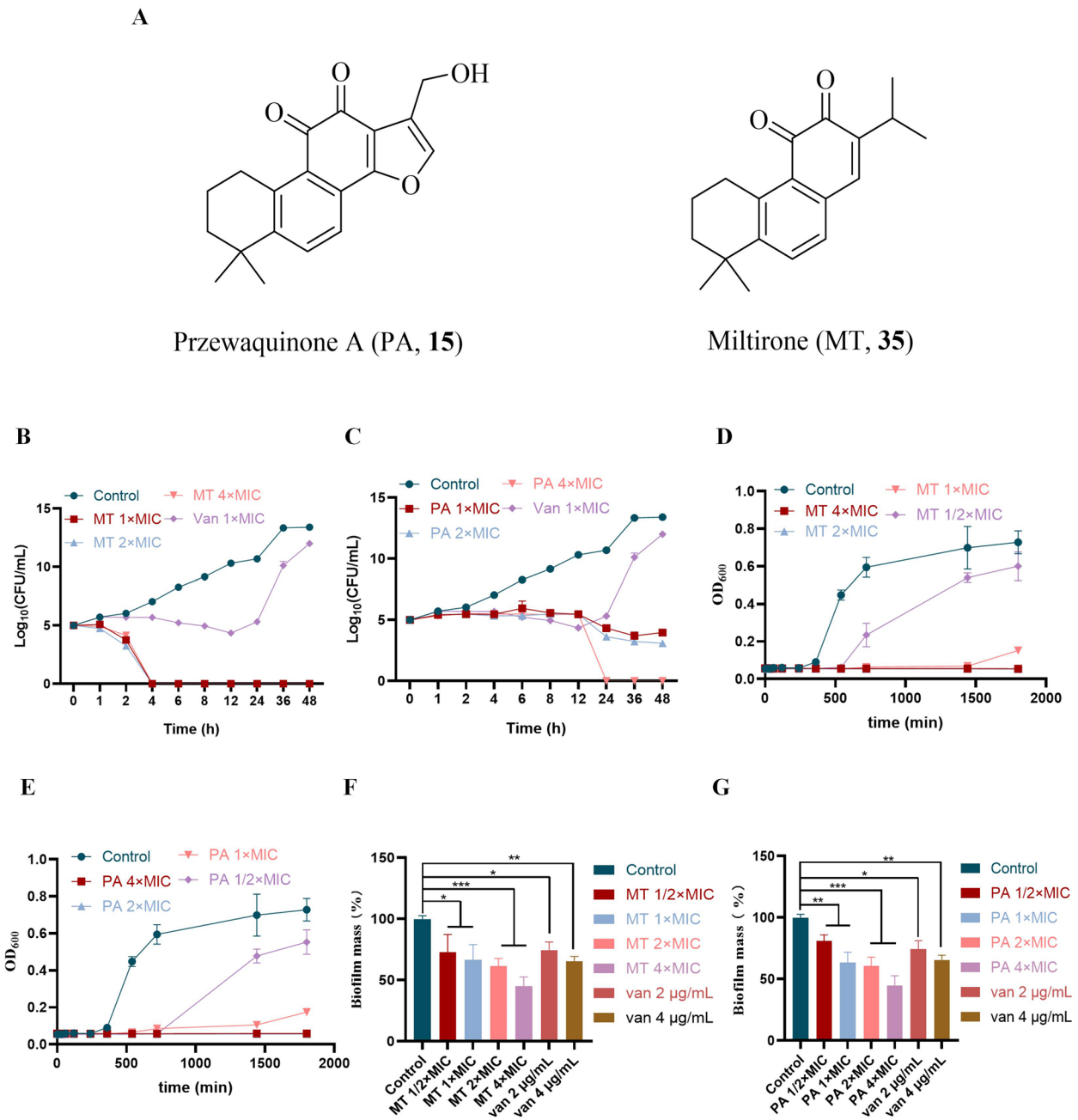


Fig. 3 **A** Structures of przewaquinone A (**15**) and miltirone (**35**). **B**, **C** Time–kill curve 1 – 4 × MIC. **D**, **E** Growth of exponential phase cultures 1/2–4 × MIC. **F**, **G** Effect of 1/2–4 × MIC on preformed biofilm. The data in the figure is represented by "mean ± standard deviation", with three replicates in each group. ****$P < 0.0001$ vs control; ***$P < 0.001$ vs control; **$P < 0.01$ vs control; *$P < 0.05$ vs control

effect on biofilm formation with best clearance effect of 55% at 4×MIC (16 μg/mL) for miltirone and 32 μg/mL for przewaquinone A (Fig. 3F, G).

Furthermore, the fluorescence microscope (FM) images showed similar results with the biofilm destroyed dependent on doses (Fig. 4A, B), in which FITC binded to proteins and nucleic acids on the bacterial surface and DAPI binded to DNA.

2.4 Miltirone and przewaquinone A targeted on cell membrane and causing leakage of contents without toxicity

MRSA003 exhibited a smooth surface and normal morphology in the control group, but showed shriveled and ruptured surfaces by miltirone and przewaquinone A treatment (Fig. 5). Then the impact of them on the integrity of cell membranes were further evaluated by measuring fluorescence intensity (Fig. 5B), which indicated the effects of miltirone and przewaquinone A on cell membrane integrity in a dose-dependent manner. Furthermore, they induced the release of β-galactosidase from MRSA003, dependent on time and concentration (Fig. 5C). In addition, membrane fluidity were changed by both compounds from fluorescent probe Laurdan (Fig. 5D), indicating disruption of basic metabolic and bacterial homeostasis. The fluorescence intensity were increased after their treatment in a dose-dependent manner (Fig. 5E), suggesting both compounds disruption of the internal positive and external negative polarization states of cell membranes, and then leading to changes in the permeability of the cell membrane. Finally, miltirone and przewaquinone A did not show any toxicity to *Galleria mellonella* larvae at treatment concentrations (Fig. 5F–G).

2.5 Effects of miltirone and przewaquinone A on the metabolome of MRSA

To elucidate underlying mechanism of miltirone and przewaquinone A, intracellular metabolomic was performed using UPLC-Q-TOF–MS, and PCA was used to conduct overall metabolic variation between samples and within each group. The PCA results showed differences in the metabolic groups (Fig. 6A), and the validation miltirone (Fig. 6B) and przewaquinone A (Fig. 6C) model were shown as follow: R2X = 0.47 and 0.54, R2Y = 0.9987 and 0.9991, Q2 = 0.8687 and 0.9503, respectively. 159 metabolites were altered significantly with 139 up-regulated and 20 down-regulated in the miltirone group, while 96 metabolites were altered significantly with 60 metabolites up-regulated and 20 metabolites

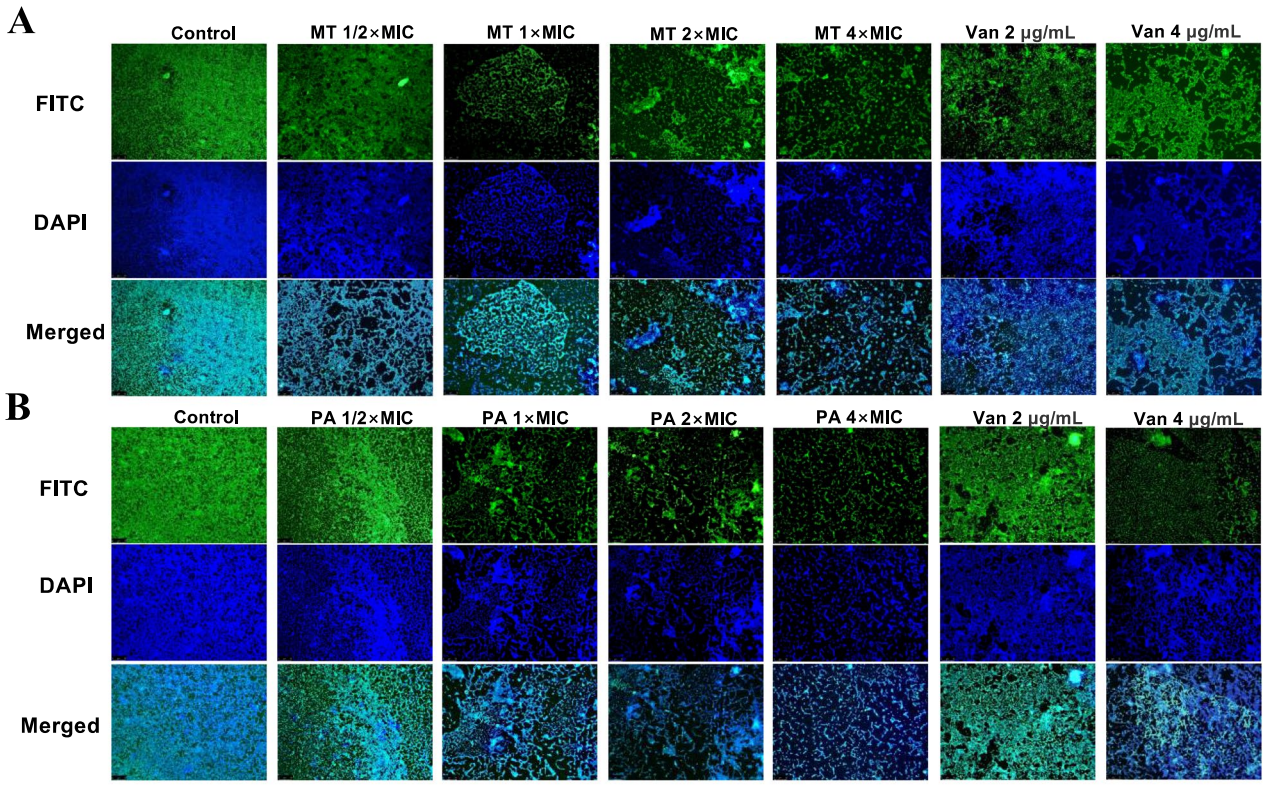


Fig. 4 **A**, **B** FM images of the MRSA00 biofilm

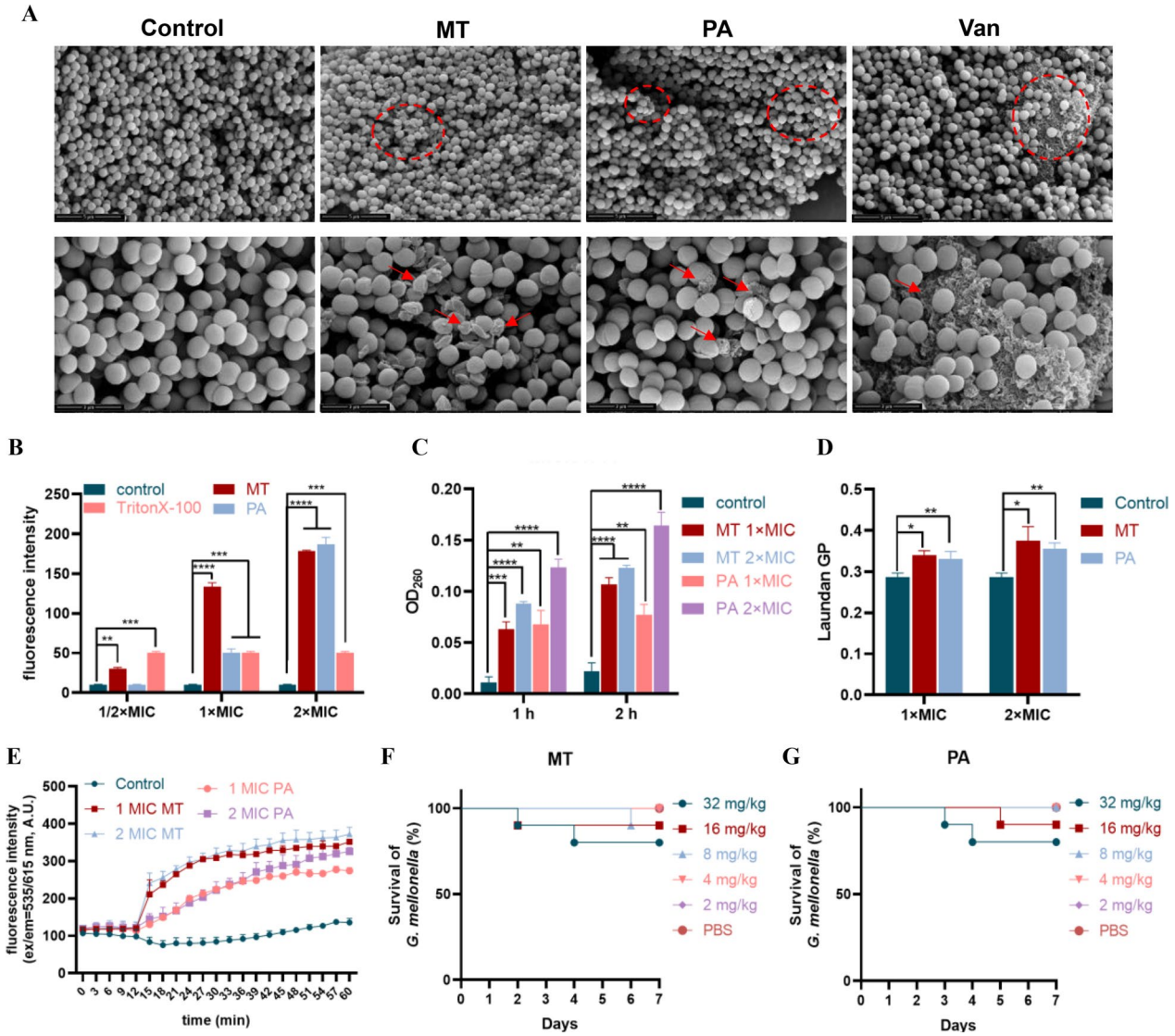


Fig. 5 **A** Effect of 4 × MIC miltirone or przewaquinone A and vancomycin on MRSA003 biofilm bacterial morphology. Scale bars in the overall and magnified images represent 5 μm and 2 μm, respectively. **B** Compounds (1/2–2 × MIC) increasing the membrane permeability of MRSA003. **C** Amount of nucleic acid leakage. D: Reducing the membrane fluidity of MRSA003. E: The membrane potential of MRSA003 after treatment. **F**–**G** The survival rate of *G. mellonella* larvae after compounds treatment. The data in the figure represented by "mean ± standard deviation", with three replicates in each group. ****$P < 0.0001$ vs control; ***$P < 0.001$ vs control; **$P < 0.01$ vs control; *$P < 0.05$ vs control

down-regulated (VIP > 1.5, FDR < 0.05)) in the przewaquinone A group. Hierarchical clustering was performed based on the top 100 differential metabolites with VIP values to observe changes in metabolites and draw a clustering heatmap for the miltirone (Fig. 6D) and przewaquinone A groups (Fig. 6E). KEGG enrichment analysis (Fig. 6F, G) suggested their influence on a wide range of metabolic pathways in MRSA.

Phosphatidylglycerol is the main component of the membrane of MRSA [20]. As shown in Fig. 5F, G, MT and PA can affect glycerolipid metabolism, which can destroy membranes and inhibit repair. This is consistent with the previous experimental results. Besides, MT and PA can affect the metabolism of multiple amino acids including cyanoamino acid metabolism, lysine biosynthesis, tyrosine metabolism, d-glutamine and d-glutamate metabolism. Amino acids are the fundamental units that make up proteins and are crucial for bacterial growth [21]. The metabolism of amino acids is affected which will affect the synthesis and repair of proteins, as well as the production of carbon and nitrogen sources within the bacteria, thereby affecting bacterial growth.

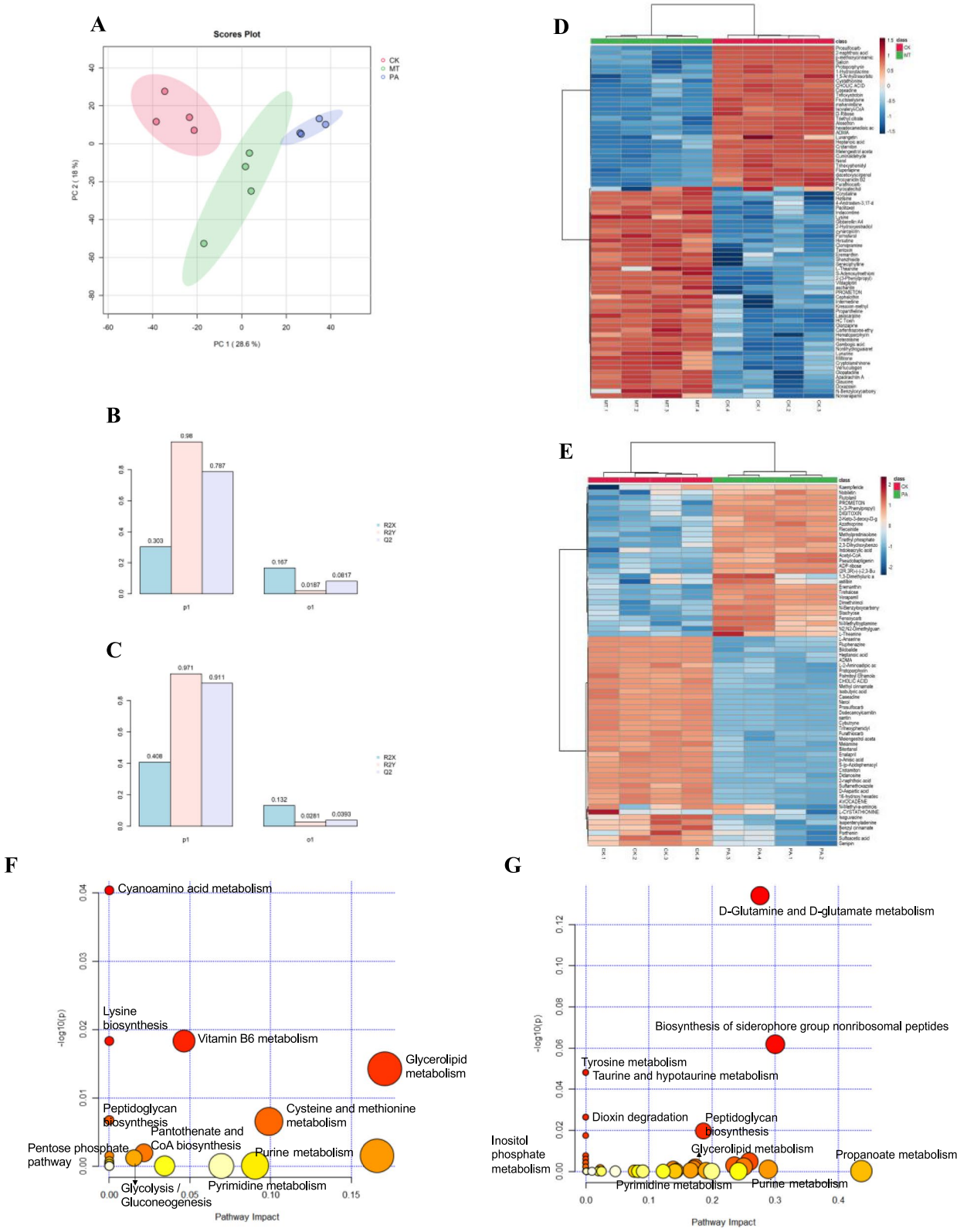


Fig. 6 Effects of miltirone and przewaquinone A on the metabolome of MRSA003. **A** Principal component analysis of the metabolome resulted in a significant separation of three groups. **B**, **C** The model validation plots (miltirone and przewaquinone A). **D**–**E** Heat-map and hierarchical clustering analysis of the metabolite differentially abundant in MRSA003 treated with miltirone (**D**) or przewaquinone A (**E**) (FDR < 0.05)). **F**, **G** KEGG enrichment analysis of metabolic pathways based differential metabolites in MRSA treated with miltirone (**F**) or przewaquinone A (**G**)

Carbohydrate metabolism is an important pathway for the energy required for bacterial activity [22]. MT and PA can impact glycolysis gluconeogenesis and various other energy metabolism pathways in this article. Specifically, changes in the external environment can also lead to disturbances in energy metabolism [22]. No matter what the reason is, some changes caused by energy metabolism disorders were found in this article. In addition, some pathways related to nucleotide metabolism are also affected such as pyrimidine metabolism and purine metabolism, which is consistent with the results of network pharmacology.

2.6 *Antibacterial effect* in vivo

Wound infection model was established to evaluate antibacterial effect miltirone in vivo (Fig. 7A), and as a result, the wound sizes were significantly reduced in the groups of 4 mg/kg and 2 mg/kg, respectively, in seven days miltirone treatment (Fig. 7B). Meanwhile, the bacterial load were reduced by miltirone treatment, roughly equal to vancomycin at same dose (Fig. 7C). In addition, the epidermis of healthy skin tissue was intact with a clear structure, and the collagen fibers in the dermis were neatly organized (Fig. 7D), but widespread necrosis of skin tissue was observed as an unstructured eosinophilic substance in the model group. Significant improvement in the skin by miltirone or vancomycin treatment were observed, with neovascularization in the dermis and subcutaneous tissue, and the thickness of surrounding epidermis at the injury sites.

3 Discussion

Salvia species are an important resource for the discovery of anti-MRSA natural medicines. In recent years, aqueous and ethanol extracts from various *Salvia* species have exhibited favorable inhibitory activity against MRSA [23], such as *S. albimaculata*. LC-HRMS analysis indicated that salvianolic acid B and homoplantaginin are the main active components [24]. In addition, the essential oil of *S. sclarea* also shows strong anti-MRSA activity [25]. However, the antibacterial potential of numerous

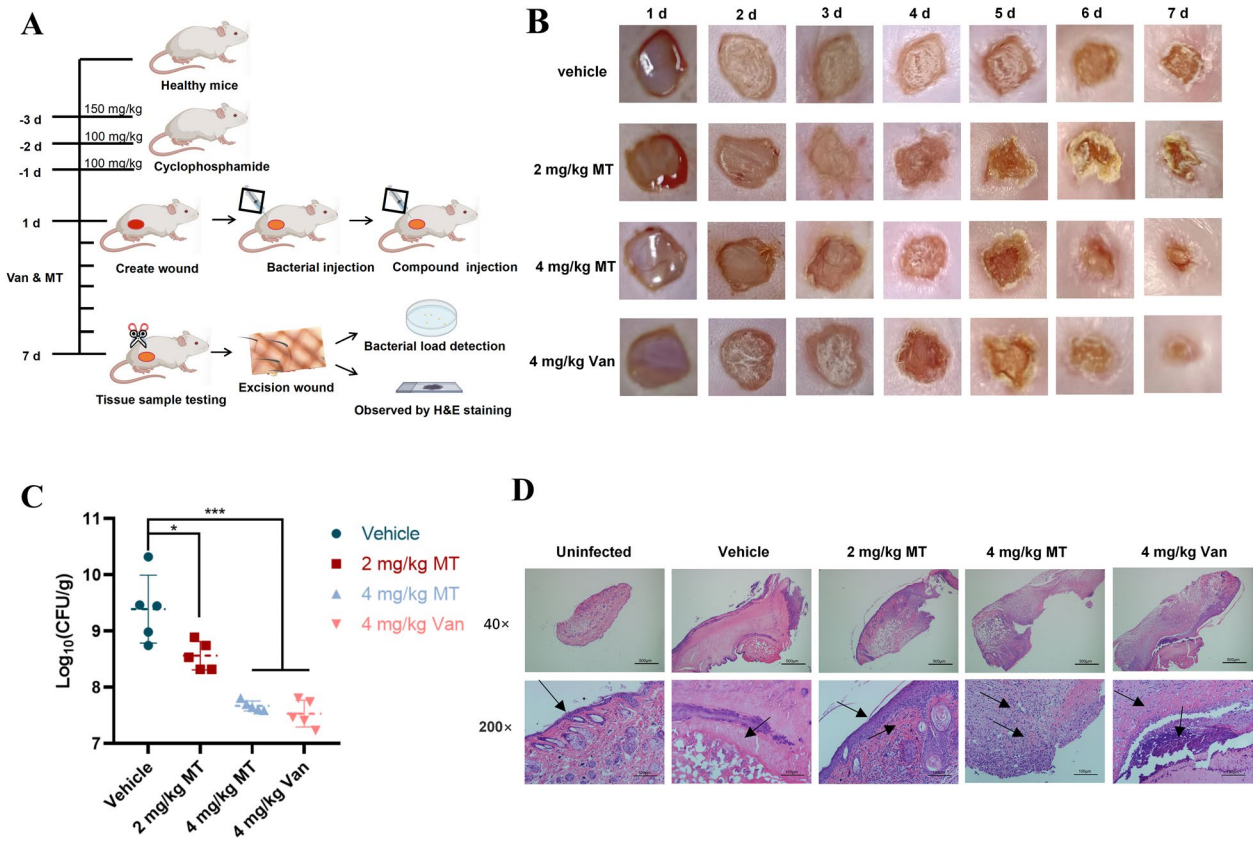


Fig. 7 **A** Schematic diagram of mice skin wound infection model. **B** Representative photographs of the wound changes of mice under the treatment of various concentrations of miltirone (2 mg/kg and 4 mg/kg) and vancomycin. **C** The bacterial load in mice skin wounds. The data in the figure represented by "mean ± standard deviation", with five replicates in each group. **D** Representative wound tissue histopathology based on H&E staining

Salvia species remains to be further investigated and exploited.

Multivariate analysis model can establish bioactive compounds correlation [10], and network pharmacology may predict potential targets interactions [11], which were used to explored anti-MRSA agents in *Salvia*. The combined strategy disclosed two unreported anti-MRSA compounds successfully, which can avoid repeating isolation of 7 plants routinely. Biofilm is a cohesive membrane layer formed by the excessive accumulation of a large number of bacteria surrounded by secreted polymers such as fibrin [26], which is difficult to eliminate and lack of target drug in market up to now [27]. Interestingly, miltirone and przewaquinone A showed scavenging effect on biofilm formation in a dose-dependent manner, respectively.

Phosphatidylglycerol is the main component of MRSA membrane [20], while carbohydrate metabolism is an important pathway for the energy required by bacteria [22]. Miltirone and przewaquinone A interfered with glycerolipid, glycolysis, gluconeogenesis, and other energy metabolic pathways, which could destroy membranes and inhibit their repair. Amino acids are fundamental units that make up proteins, and are crucial for bacterial growth [21]. Miltirone and przewaquinone A significantly influenced the metabolic pathway of various amino acids in MRSA by metabolomic analysis, which in turn might impair the synthesis and repair of proteins, as well as the production of carbon and nitrogen sources within bacteria, then affecting bacterial growth. The cell membrane serves as a vital protective barrier for cell, and its biophysical integrity and functionality are of paramount importance for bacterial growth and survival [28]. Miltirone and przewaquinone A could interfere with cell membrane function, resulting in the release of cellular contents and ultimately leading to the death of MRSA, respectively.

MRSA infections hinder wound healing [29], and bacterial colonization within wounds can reduce oxygen availability, thus preventing tissue regeneration. Then, effective management of bacterial infection is an essential prerequisite character for the successful treatment of wounds [30]. In our research, miltirone can improve wound healing in murine model, and concurrently mitigate bacterial colonization of wounds, showing roughly therapeutic effects as vancomycin.

In summary, two unreported anti-MRSA compounds from *Salvia* plants were revealed quickly and effectively using the combination of multivariate analysis and network pharmacology, and then their efficacy and pathway were validated by serial experiments in vitro and in vivo. The finding supported the traditional use of *Salvia* plants, and then presented miltirone and przewaquinone A as bactericide and biofilm scavenger, which should be attractive to chemists and biologists.

4 Materials and methods

4.1 Plant material

All air-dried plants were collected by the Kunming Zhifen Biotechnology Company from Yunnan Province in June 2020. Authentication of the plant material was also carried out by the company and checked at http://www.theplantlist.org. Voucher specimens have been deposited in the Plant Resource Library of the College of Pharmacy, Yunnan University.

4.2 Strains, chemicals, reagents, and Galleria mellonella

The clinical isolates of MRSA003 were obtained from the First People's Hospital of Zunyi City. *Staphylococcus aureus* ATCC 25923 (MSSA), Multidrug-resistant (MDR) strains of *Enterococcus faecalis* (VRE, ATCC 51299), *Acinetobacter baumannii* (Bio-53272), and *Pseudomonas aeruginosa* (Bio-109004) were purchased from Beijing Bio-Bridge Technology Co., Ltd, China. MDR *Escherichia coli* (YIM B01141) was obtained from the Yunnan Institute of Microbiology. Mass-grade methanol, acetonitrile, isopropanol and formic acid were purchased from Merck. Watson's water was purchased from Watsons Food and Beverage Co., Ltd. Dimethylsulfoxide (DMSO), TSA, TSB, PBS, vancomycin, ampicillin, cefoxitin, polymyxin B sulfate, polyformaldehyde, fluorescein isothiocyanate isomer (FITC), 4',6-diamidino2-phenylindole (DAPI), isoamyl acetate, propidium Iodide (PI), 3,3'-dipropylthiadicarbocyanine iodide (DiSC3 [5]), and the Laurdan probe were purchased from Macklin Reagents (Shanghai, China). All standard compounds including przewaquinone A and miltirone (purity ≥ 98%) were obtained from Le Mei Tian (ChenDu, China). *Galleria mellonella* larvae were obtained from Huiyude Biotechnology Co., Ltd., China.

4.3 Animals

Specific pathogenic-free female ICR mice (weight ranged from 16 to 23 g) were obtained from Kunming Medical University. All mice were raised in a laboratory of specific pathogen-free (SPF) level at room temperature (20–25℃) with a standard diet and water, constant humidity (40–70%), and a 12-h/12-h light–dark cycle. In accordance with international guidelines for animal experimentation and internationally recognized ethical principles for the use and care of experimental animals, the animal study was approved by the Institutional Animal Care and Use Committee of Yunnan University (animal ethics approval code: YNUCARE202210020).

4.4 Preparation of extracts

The dried herbs were processed as described in the Supplementary Material (S1). Subsequently, all fractions were tested for anti-MRSA effect, resulting in the identification of nine bioactive fractions. Minimum inhibitory concentration (MIC) data were presented in Table S2, and the components yields were listed in Table S3.

4.5 UPLC-Q-TOF–MS analysis and multivariate analysis

Chromatographic separation and mass spectral data of the fractions were obtained using ultra-high-performance liquid chromatography (UPLC) with a 6545 Q-TOF–MS system (Agilent Technologies, Palo Alto, CA, USA), and the instrument parameters were listed in the Supplementary Material (S2). Principal component analysis (PCA) was conducted using Origin software (Version 8.0) on 9 bioactive fractions from 7 plants to explore the correlation between *Salvia* extracts and anti-MRSA bioactivity.

4.6 Network pharmacology

Network pharmacology analysis followed the literatures [11, 31] with a few modifications with details in the Supplementary Materia (S3).

4.7 Antimicrobial bioactivity

4.7.1 Determination of the MIC and MBC

In accordance with the Clinical and Laboratory Standards Institute protocols (CLSI, 2021), the MIC and MBC of miltirone and przewaquinone A were determined using the broth microdilution method [32] in the Supplementary Material (S4).

4.7.2 Time–kill curve

The time-kill curves of miltirone and przewaquinone A against MRSA003 were analyzed as previously described [33] with details in Supplementary Material (S5).

4.7.3 Growth kinetics

Growth kinetic assay was used to assess MRSA003 growth and death [34], as described in the Supplementary Material (S6).

4.7.4 Antibiofilm assay

Quantitative analysis of the biofilms was performed using the crystal violet method, and biofilm observation was carried out using a fluorescence microscope following the literatures [3, 29], as described in Supplementary Material (S7).

4.7.5 Scanning electron microscope

Field-emission scanning electron microscopy (SEM; Nova Nano SEM 450, FEI, USA) was used to observe the effects of miltirone and przewaquinone A against MRSA003 [35] with details in Supplementary Material (S8).

4.7.6 Cell membrane integrity assay

The integrity of the MRSA003 membrane was evaluated using PI [28] in Supplementary Material (S9).

4.7.7 Cell membrane depolarization assay

3,3'-dipropylthiadicarbocyanine iodide (DiSC3 [5]) (Maokang Biotechnology Co., Ltd., Shanghai, China) was used to assess the membrane depolarization status of MRSA003 [36] with details in Supplementary Material (S10).

4.7.8 Evaluation of membrane fluidity

Membrane fluidity was evaluated with a Laurdan probe [28, 37] with details in Supplementary Material (S11).

4.7.9 Nucleic acid leakage

The impact of miltirone and przewaquinone A on cell permeability were evaluated by quantifying the release of nucleic acids from cells into the medium [38] with detailed information in the Supplementary Material (S12).

4.7.10 Cytotoxicity in vivo

G. mellonella was used to evaluate the cytotoxicity of miltirone and przewaquinone A in vivo [38, 39], with the specific experimental procedure in Supplementary Material (S13).

4.7.11 Metabolomics analysis

MRSA003 was adjusted to a density of 1×10^7 CFU/ml after culturing to the growth logarithmic phase and incubated for 4 h at 37 °C after treatment with or without 1/2×MIC miltirone or przewaquinone A [40]. The MRSA003 metabolites were extracted and derivatized according to a previously described method [29], and detailed experimental procedures was provided in the Supplementary Material (S14).

4.7.12 Mice skin wound infection model

A mouse skin wound infection model was established to determine anti-MRSA bioactivity in vivo and the capacity to facilitate the wound healing process [29, 41], and the details were provided in Supplementary Material (S15).

4.8 Data analysis

All assays were performed in triplicate and repeated three times independently. Data were analyzed by variance and the significance of the difference was evaluated with a Tukey's test ($p \leq 0.05$). Statistical analyses were

performed using GraphPad Prism software (v.6.0; GraphPad Software, CA, USA). Multivariate statistical analyses of principal component analysis (PCA) and heatmaps were generated by Origin 2021 software (OriginLab, Northampton, MA, USA).

Abbreviations

CDC	Centers for Disease Control and Prevention
CFU	Colony-forming unit assays
DAPI	4′,6-Diamidino-2-Phenylindole
FITC	Fluorescein isothiocyanate
MIC	Minimum inhibitory concentration
MBC	Minimum bactericidal concentration
PBS	Phosphate buffered solution
PCA	Principal component analysis
PPI	Protein–protein interaction
SEM	Scanning electron microscope
TIC	Total ion chromatograms
TSA	Tryptic soy agar
TSB	Tryptic soy broth
KEGG	Kyoto Encyclopedia of Genes and Genomes
GO	Gene Ontology
MT	Miltirone
PA	Przewaquinone A

Supplementary Information

The online version contains supplementary material available at https://doi.org/10.1007/s13659-026-00624-0.

Supplementary Material 1.

Acknowledgements
This work was financially supported partly by the National Natural Science Foundation of China (U2202212), the High-level Talent Promotion and Training Project of Kunming (grant numbers 2022SCP003), Project of Yunnan Characteristic Plant Screening and R&D Service CXO Platform (grant numbers 2022YKZY001). The authors would like to thank the Advanced Analysis and Measurement Center of Yunnan University for their technical support.

Author contributions
Xiao-Dong Luo: Conceptualization, Writing—Review & Editing, Supervision. Huan Huang: Methodology, Validation, Formal analysis, Investigation, Writing—Original Draft, Visualization. Zhao-Jie Wang: Conceptualization, Writing—Review & Editing, Project administration. Li-Yu Bai: Methodology, Investigation, Data Curation. Yue-Ming Jiang: Investigation. Yan-Yan Zhu: Methodology. All the authors made substantial contributions to the results and editing of the manuscript. The authors read and approved the final manuscript.

Funding
National Natural Science Foundation of China, U2202212, Xiao-Dong Luo, High-level Talent Promotion and Training Project of Kunming, 2022SCP003, Xiao-Dong Luo, Yunnan Characteristic Plant Screening and R&D Service CXO Platform, 2022YKZY001, Xiao-Dong Luo.

Data availability
The data supporting the results of this study can be obtained from the corresponding author on reasonable request.

Declarations

Competing interests
The authors declare that they have no conflict of interest.

Author details
[1]Yunnan Characteristic Plant Extraction Laboratory, Key Laboratory of Medicinal Chemistry for Natural Resource, Ministry of Education and Yunnan Province, School of Chemical Science and Technology, Yunnan University, Kunming 650500, People's Republic of China. [2]State Key Laboratory of Phytochemistry and Plant Resources in West China, Kunming Institute of Botany, Chinese Academy of Sciences, Kunming 650201, People's Republic of China.

Received: 17 January 2026 Accepted: 3 March 2026
Published online: 01 June 2026

References

1. Ding CF, Zhang RP, Yu HF, Yang J, Qin XJ, Dai Z, et al. Hybrid isoquinolines from *Thalictrum foetidum*: a new type of aporphine inhibiting *Staphylococcus aureus* by combined mechanisms. Org Chem Front. 2019;6:3428–34. https://doi.org/10.1039/c9qo00737g.
2. Wei X, Yang J, Ma H-X, Ding C-F, Yu H-F, Zhao Y-L, et al. Antimicrobial indole alkaloids with adductive C_9 aromatic unit from *Gelsemium elegans*. Tetrahedron Lett. 2018;59:2066–70. https://doi.org/10.1016/j.tetlet.2018.04.041.
3. Wu X, Ma GL, Chen HW, Zhao ZY, Zhu ZP, Xiong J, et al. Antibacterial and antibiofilm efficacy of the preferred fractions and compounds from *Euphorbia humifusa* (herba euphorbiae humifusae) against *Staphylococcus aureus*. J Ethnopharmacol. 2023;306:116177. https://doi.org/10.1016/j.jep.2023.116177.
4. Yang X, Gao X, Ou J, Chen G, Ye L. Antimicrobial activity and mechanism of anti-MRSA of phloroglucinol derivatives. Daru J Pharm Sci. 2024. https://doi.org/10.1007/s40199-024-00503-4.
5. Sartorius B, Gray AP, Weaver ND, Aguilar GR, Swetschinski LR, Ikuta KS, et al. The burden of bacterial antimicrobial resistance in the WHO African region in 2019: a cross-country systematic analysis. Lancet. 2024;12:e201–16. https://doi.org/10.1016/s2214-109x(23)00539-9.
6. Yu HF, Huang WY, Ding CF, Wei X, Zhang LC, Qin XJ, et al. Cage-like monoterpenoid indole alkaloids with antimicrobial activity from *Alstonia scholaris*. Tetrahedron Lett. 2018;59:2975–8. https://doi.org/10.1016/j.tetlet.2018.06.047.
7. Zhao LY, Liu HX, Wang L, Xu ZF, Tan HB, Qiu SX. Rhodomyrtosone B, a membrane-targeting anti-MRSA natural acylgphloroglucinol from *Rhodomyrtus tomentosa*. J Ethnopharmacol. 2019;228:50–7. https://doi.org/10.1016/j.jep.2018.09.011.
8. Liang CL, Wang L, Lei J, Duan BZ, Ma WS, Xiao SM, et al. A Comparative analysis of the chloroplast genomes of four *Salvia* medicinal plants. Engineering. 2019;5:907–15. https://doi.org/10.1016/j.eng.2019.01.017.
9. Robinson JL, Salvadori MI, Canadian Paediat S. Management of community-associated methicillin-resistant *Staphylococcus aureus* skin abscesses in children. Paediatr Child Health. 2011;16:115–6. https://doi.org/10.1093/pch/16.2.115.
10. Wang ZJ, Zhou Y, Shi XL, Xia X, He YJ, Zhu YY, et al. Comparison of chemical constituents in diverse zanthoxylum herbs, and evaluation of their relative antibacterial and nematicidal activity. Food Biosci. 2021. https://doi.org/10.1016/j.fbio.2021.101206.
11. Deng X, Lei HY, Ren YS, Ai J, Li YQ, Liang S, et al. A novel strategy for active compound efficacy status identification in multi-tropism Chinese herbal medicine (*Scutellaria baicalensis* Georgi) based on multi-indexes spectrum-effect gray correlation analysis. J Ethnopharmacol. 2023;300:115677. https://doi.org/10.1016/j.jep.2022.115677.
12. Liu AH, Lin YH, Yang M, Guo H, Guan SH, Sun JH, et al. Development of the fingerprints for the quality of the roots of *Salvia miltiorrhiza* and its related preparations by HPLC-DAD and LC-MS(n). J Chromatogr B Anal Technol Biomed Life Sci. 2007;846:32–41. https://doi.org/10.1016/j.jchromb.2006.08.002.
13. Yang ST, Wu X, Rui W, Guo J, Feng YF. UPLC/Q-TOF-MS Analysis for Identification of Hydrophilic Phenolics and Lipophilic Diterpenoids from Radix *Salviae Miltiorrhizae*. Acta Chromatogr. 2015;27:711–28. https://doi.org/10.1556/AChrom.27.2015.4.9.
14. Parejo I, Jauregui O, Sanchez-Rabaneda F, Viladomat F, Bastida J, Codina C. Separation and characterization of phenolic compounds in fennel (*Foeniculum vulgare*) using liquid chromatography-negative electrospray ionization tandem mass spectrometry. J Agric Food Chem. 2004;52:3679–87. https://doi.org/10.1021/jf030813h.
15. Dai H, Wang M, Li X, Wang L, Li Y, Xue M. Structural elucidation of *in vitro* and *in vivo* metabolites of cryptotanshinone by HPLC-DAD-ESI-MS(n). J

Pharm Biomed Anal. 2008;48:885–96. https://doi.org/10.1016/j.jpba.2008.07.011.
16. Ge P, Wen L, Wang X, Zhang J, Xu G. Rapidly identify compounds from danshen by using ultra-high-performance liquid chromatography coupled with linear ion trap-Orbitrap mass spectrometer and predict its mechanisms of intervening thrombotic diseases. J Liq Chromatogr Relat Technol. 2019;42:115–21. https://doi.org/10.1080/10826076.2018.1511993.
17. Lin Z, Qiu S, Wufuer A, Shum L. Simultaneous determination of glycyrrhizin, a marker component in radix Glycyrrhizae, and its major metabolite glycyrrhetic acid in human plasma by LC–MS/MS. J Chromatogr B Anal Technol Biomed Life Sci. 2005;814:201–7. https://doi.org/10.1016/j.jchromb.2004.10.026.
18. Wang M, Dai H, Li X, Li Y, Wang L, Xue M. Structural elucidation of metabolites of tanshinone I and its analogue dihydrotanshinone I in rats by HPLC-ESI-MSn. J Chromatogr B Anal Technol Biomed Life Sci. 2010;878:915–24. https://doi.org/10.1016/j.jchromb.2010.02.014.
19. Guan F, Uboh CE, Soma LR, Luo Y, Rudy J, Tobin T. Detection, quantification and confirmation of anabolic steroids in equine plasma by liquid chromatography and tandem mass spectrometry. J Chromatogr B Anal Technol Biomed Life Sci. 2005;829:56–68. https://doi.org/10.1016/j.jchromb.2005.09.045.
20. Zhu YY, Wang ZJ, Zhu M, Zhou ZS, Hu BY, Wei MZ, et al. A dual mechanism with H2S inhibition and membrane damage of morusin from *Morus alba* Linn. against MDR-MRSA. Bioorg Med Chem. 2024;97:117544. https://doi.org/10.1016/j.bmc.2023.117544.
21. Dan W, Gao J, Zhang J, Cao Y, Liu J, Sun Y, et al. Antibacterial activity and mechanism of action of canthin-6-one against *Staphylococcus aureus* and its application on beef preservation. Food Control. 2023. https://doi.org/10.1016/j.foodcont.2023.109604.
22. Liu M, Feng M, Yang K, Cao Y, Zhang J, Xu J, et al. Transcriptomic and metabolomic analyses reveal antibacterial mechanism of astringent persimmon tannin against Methicillin-resistant *Staphylococcus aureus* isolated from pork. Food Chem. 2020;309:125692. https://doi.org/10.1016/j.foodchem.2019.125692.
23. Doctor LAH, Cachón AHU, Beh AD, Sánchez AAG, León JAA, Salinas GMM, et al. Chemometric and dereplication analyses of the anti-staphylococcus aureus strains activity of *Salvia hispanica* L. seeds. J Med Food. 2025;28:615–24. https://doi.org/10.1089/jmf.2024.0241.
24. Tütüniş SY, Toraman GÖA, Dincel ED, Tufan S, Akalın E, Tan E, et al. In silico and *in vitro* antibacterial evaluation of eight Anatolian *Salvia* species with chemical profiling by LC-HRMS. Sci Rep. 2025;15:31404–31404. https://doi.org/10.1038/s41598-025-15803-1.
25. Mendil AL, Amarni M, Chelghoum H, Lacheheb S, Moussa H, Aboumustapha M, et al. Essential oil from aerial parts of *Salvia sclarea:* A comprehensive study of antibacterial activity through chemical profiling, molecular interactions, and predictive modeling using QSARKNNPCA. J Essent Oil Bear Plants. 2025;28:902–19. https://doi.org/10.1080/0972060x.2025.2559656.
26. Zeng Q, Wang ZJ, Chen S, Wang H, Xie TZ, Xu XJ, et al. Phytochemical and anti-MRSA constituents of *Zanthoxylum nitidum*. Biomed Pharmacother. 2022;148:112758. https://doi.org/10.1016/j.biopha.2022.112758.
27. Du H, Zhou L, Lu Z, Bie X, Zhao H, Niu YD, et al. Transcriptomic and proteomic profiling response of methicillin-resistant *Staphylococcus aureus* (MRSA) to a novel bacteriocin, plantaricin GZ1-27 and its inhibition of biofilm formation. Appl Microbiol Biotechnol. 2020;104:7957–70. https://doi.org/10.1007/s00253-020-10589-w.
28. Song M, Liu Y, Li T, Liu X, Hao Z, Ding S, et al. Plant natural flavonoids against multidrug resistant pathogens. Adv Sci. 2021;8:e2100749. https://doi.org/10.1002/advs.202100749.
29. Liu T, Wang Z-J, Shi Y-Z, Tao R, Huang H, Zhao Y-L, et al. Curcusinol from the fruit of *Carex baccans* with antibacterial activity against multidrug-resistant strains. J Ethnopharmacol. 2023;318:116892–116892. https://doi.org/10.1016/j.jep.2023.116892.
30. Jin X, Shan J, Zhao J, Wang T, Zhang W, Yang S, et al. Bimetallic oxide Cu-Fe_3O_4 nanoclusters with multiple enzymatic activities for wound infection treatment and wound healing. Acta Biomater. 2024;173:403–19. https://doi.org/10.1016/j.actbio.2023.10.028.
31. Gu K, Feng S, Zhang X, Peng Y, Sun P, Liu W, et al. Deciphering the antifungal mechanism and functional components of *cinnamomum cassia* essential oil against *Candida albicans* through integration of network-based metabolomics and pharmacology, the greedy algorithm, and molecular docking. J Ethnopharmacol. 2024;319:117156. https://doi.org/10.1016/j.jep.2023.117156.
32. Wang XN, Wang ZJ, Zhao Y, Wang H, Xiang ML, Liu YY, et al. Antifungal alkaloids from *Mahonia fortunei* against pathogens of postharvest fruit. Nat Prod Bioprospect. 2023;13:10. https://doi.org/10.1007/s13659-023-00374-3.
33. Klepser ME, Ernst EJ, Lewis RE, Ernst ME, Pfaller MA. Influence of test conditions on antifungal time-kill curve results: proposal for standardized methods. Antimicrob Agents Chemother. 1998;42:1207–12. https://doi.org/10.1128/aac.42.5.1207.
34. Nye TM, Tukenmez H, Singh P, Flores-Mireles AL, Obernuefemann CLP, Pinkner JS, et al. Ring-fused 2-pyridones effective against multidrug-resistant Gram-positive pathogens and synergistic with standard-of-care antibiotics. Proc Natl Acad Sci U S A. 2022;119:e2210912119–e2210912119. https://doi.org/10.1073/pnas.2210912119.
35. Ma DY, Wang ZJ, Chen YC, Qi ZH, Wang H, Zhu YY, et al. Antifungal compounds of Chinese prickly ash against drug-resistant *Candida albicans*. Food Chem X. 2022;15:100400. https://doi.org/10.1016/j.fochx.2022.100400.
36. Cheng W, Xu T, Cui L, Xue Z, Liu J, Yang R, et al. Discovery of amphiphilic xanthohumol derivatives as membrane-targeting antimicrobials against methicillin-resistant *Staphylococcus aureus*. J Med Chem. 2023;66:962–75. https://doi.org/10.1021/acs.jmedchem.2c01793.
37. Sun L, Tang Z, Wang M, Shi J, Lin Y, Sun T, et al. Exploration of antimicrobial ingredients in *Psoralea corylifolia* L. Seed and related mechanism against methicillin-resistant *Staphylococcus aureus*. Molecules. 2022;27:6952. https://doi.org/10.3390/molecules27206952.
38. Zhang C, Wang L, Deng W, Huang H, Wang J, Liao X, et al. Metal-ruthenium complex based on dipyridylamine group as membrane-active antibacterial agent effectively decrease the development of drug-resistance on *Staphylococcus aureus*. J Inorg Biochem. 2023. https://doi.org/10.1016/j.jinorgbio.2023.112385.
39. Furtado AA, Daniele-Silva A, de Oliveira IR, Mendes RF, Dos Santos EC, de Carvalho E, et al. *In silico* and *in vitro* structure-stability-function relationship of analog peptides of Stigmurin and its antibacterial and antibiofilm activities. Pharmacol Res. 2022;181:106245. https://doi.org/10.1016/j.phrs.2022.106245.
40. Ma M, Zhao J, Zeng Z, Yu P, Xia J, Wan D, et al. Deciphering the antibacterial mechanism of monocaprin against methicillin-resistant *Staphylococcus aureus* by integrated transcriptomic and metabolomic analyses and its application in pork preservation. Lwt. 2023. https://doi.org/10.1016/j.lwt.2023.114569.
41. Dai JK, Dan WJ, Cao YD, Gao JX, Wang JR, Wan JB. Discovery of new quaternized norharmane dimers as potential anti-MRSA agents. J Adv Res. 2023. https://doi.org/10.1016/j.jare.2023.11.005.

Publisher's Note

Springer Nature remains neutral with regard to jurisdictional claims in published maps and institutional affiliations.